Dynamic control of optical response in layered metal Chalcogenide nanoplates

Yanping Liu[1], Kyle Tom[1,2], Xi Wang[1], Chunming Huang[1], Hongtao Yuan[3, 4], Hong Ding[5], Changhyun Ko[1], Joonki Suh[1], Lawrence Pan[1], Kristin A. Persson[1,5] and Jie Yao [1,2,*]

1. *Department of Materials Science and Engineering, University of California, Berkeley, California 94720, United States*
2. *Materials Sciences Division, Lawrence Berkeley National Laboratory, Berkeley, CA, 94720, USA*
3. *Geballe Laboratory for Advanced Materials, Stanford University, Stanford, California 94305, USA*
4. *Stanford Institute for Materials and Energy Sciences, SLAC National Accelerator Laboratory, Menlo Park, California 94025, USA*
5. *Environmental Energy Technologies Division, Lawrence Berkeley National Laboratory, Berkeley, CA, 94720, USA*

SUPPLEMENTARY INFORMATION

*Corresponding author: Email: yaojie@berkeley.edu

SI I. Materials Synthesis and Device Fabrication

Bi_2Se_3 single crystals were synthesized by solvothermal synthesis, the details of which were described in the main text. The other layered structure multilayer flakes were prepared using mechanical exfoliation. Experiments were performed on the layered structure nanomaterials using electrical devices fabricated on their surface. The devices were fabricated using conventional photolithography and e-beam deposition techniques, processes with micrometer scale accuracy. The thicknesses of the multiple samples were determined using optical and AFM imaging techniques. The device configurations of Bi_2Se_3 nanoplates and the other layered structure flakes measured in this study were typically 50 μm wide and 30 μm long. Reactive ion etching was performed prior to the deposition of gold electrodes. The electrodes were deposited by e-beam evaporation (5 nm Cr, 100 nm Au) patterned via standard photolithography procedures.

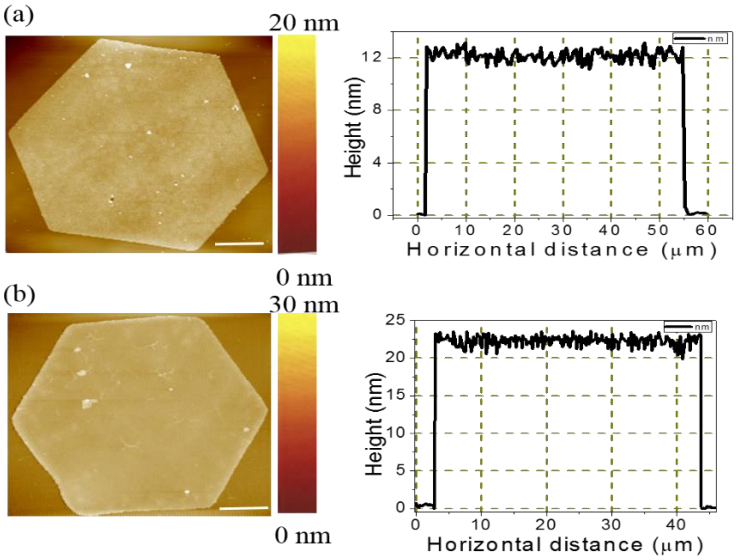

Supplementary **Figure S**1. Atomic force microscopy (AFM) image of the Bi_2Se_3 nanoplates. Line profile across the AFM image in **(a)** and **(b)**, which shows a clear value of around 12 nm and 22 nm for the two nanoplate thickness. Scale bar, 10 μm.

SI II. Identification of Materials by Raman Spectroscopy

All of the studied layered structure materials were identified using a Micro-Raman spectrometer (LabRAM HR Evolution, HORIBA)) in the scattering configuration excited with laser wavelength λ = 473 nm. A typical Raman spectrum consisting of different peaks is shown in Fig.S2, where the corresponding peak locations agree well with the reported Raman spectrum of Bi_2Se_3 nanoplates and $MoSe_2$ [1-4].

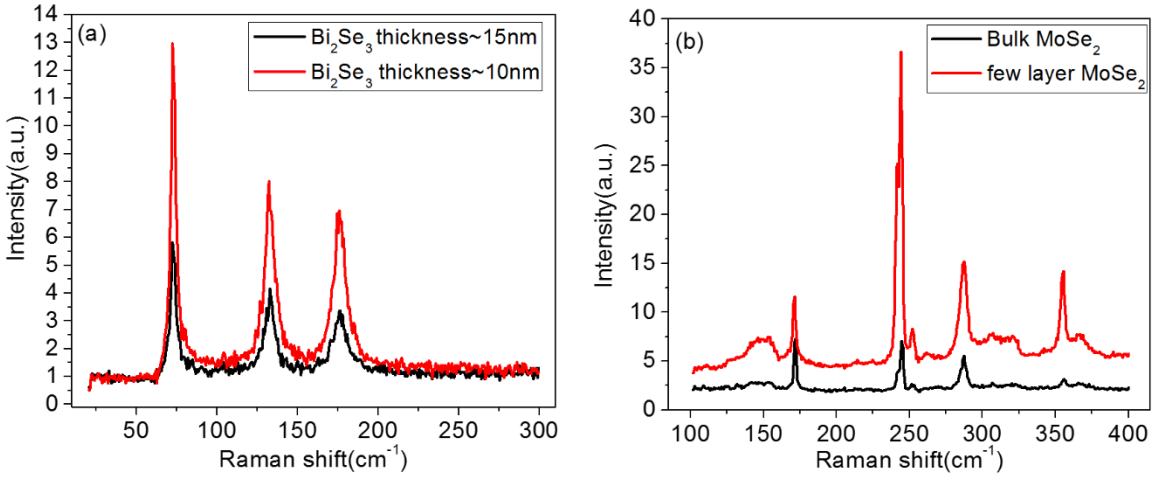

Supplementary **Figure S**2. Raman spectra of few quintuple layer (FQL) Bi_2Se_3 nanoplates **(a)** and $MoSe_2$ **(b)** in the 10-450 cm^{-1} region. The corresponding peak locations are consistent with the reported Raman spectrum of Bi_2Se_3 nanoplates and $MoSe_2$.

SI III. Characterization of the Crystal Structure of Bi_2Se_3 Nanoplates

To confirm the crystallinity of the Bi_2Se_3 nanoplates, we performed transmission electron microscopy (TEM). Fig.S3 **(a)** is a typical low magnification TEM image of the Bi_2Se_3 nanoplates. The electron diffraction results (shown in Fig. S3 **(b)**) demonstrates the single crystalline nature of the nanoplates [5].

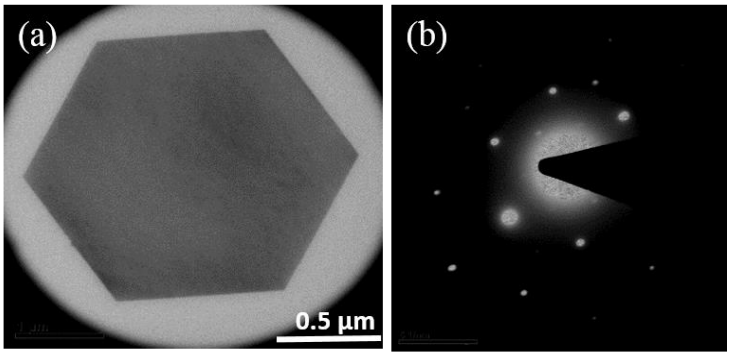

Supplementary **Figure S**3. **(a)** TEM image and **(b)** electron diffraction pattern of a Bi_2Se_3 nanoplate.

SI IV. Numerical calculation of reflectivity based on Drude model

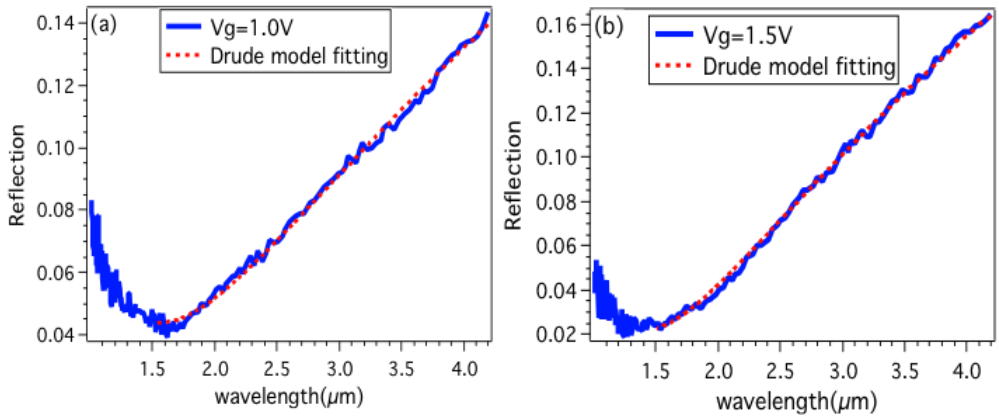

Supplementary **Figure S4**. Reflection spectra fitted with Drude model. Experimentally measured reflectance (blue) for a Bi_2Se_3 nanoplate with different ILG voltage and Numerical fitting (red) based on Drude model.

To better study the dynamic plasma frequency of Bi_2Se_3 nanoplates under ILG modulation, we applied the Drude model to our measured results and found that it perfectly fits with the experimental data (seen in Figure S4). The value of the plasma frequency can be obtained from the numerical fitting of each curve. For example, the plasma frequency reaches $\omega_p = 3.12\times10^{15}/s$, with best fit parameters $\varepsilon_\infty = 9.1$ and $\Gamma = 2.1\times10^{14}/s$, at the bias voltage

$V_G = 1.5V$, which yields an extremely high free electron concentration on the order of 10^{20} cm^{-3}. This level of electron concentration modulation is one of the great advantages of using the EDL with 2D material systems.

SI V. Numerical calculation of relative permittivity

To better interpret the dynamic optical response of Bi_2Se_3 nanoplates under ILG modulation, we calculate the relative permittivity (ϵ) of Bi_2Se3 under the bias of the ILG voltage. We found that at low frequency regions ($\omega s << 1$), $\mathrm{Re}(\varepsilon) << \mathrm{Im}(\varepsilon)$, shown in Figure S5. We observe that $\mathrm{Re}(\varepsilon)$ generally decreases with increasing plasma frequency, representative of the increasing free electron concentration. On the other hand, $\mathrm{Im}(\varepsilon)$ shows the opposite trend with increasing plasma frequency. This is expected from the Drude model when the carrier density is extremely high. The dramatic change of $\mathrm{Im}(\varepsilon)$ is primarily due to the huge free electron absorption, which comes from ILG modulation. Such behavior further identifies the increasing amount of free electrons induced by the ILG inside the materials.

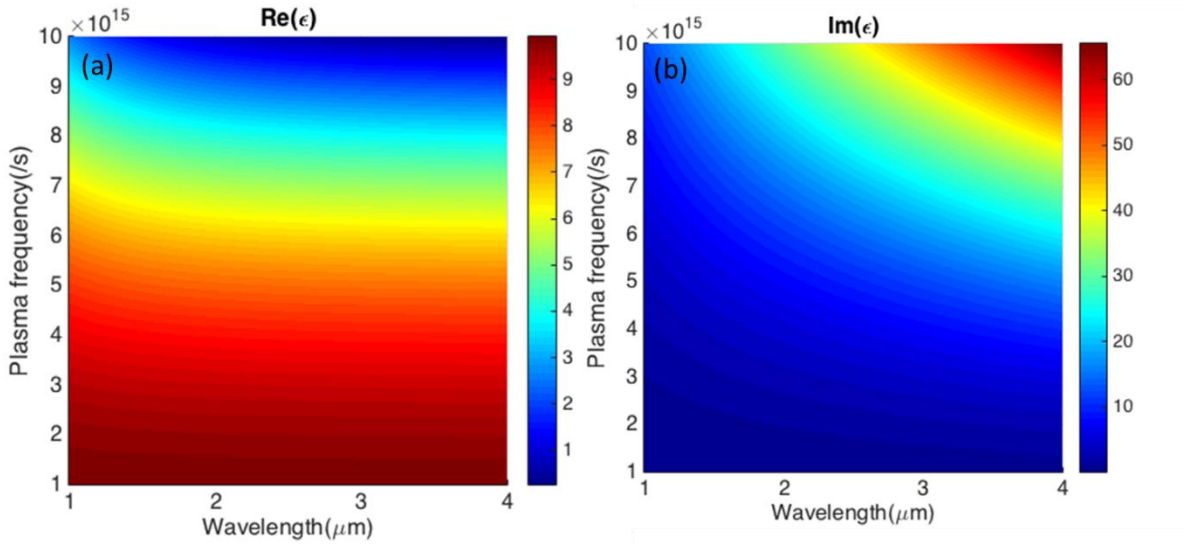

Supplementary **Figure 5**. **(a)** Real part Re(ε) and **(b)** imaginary part Im(ε) of the relative permittivity as functions of the plasma frequency induced by the ILG modulation. The calculated Im(ε) increases with the increasing plasma frequency at long wavelengths. The simulated parameters based on the experimental reflection spectra: $\Gamma = 2.1\times10^{14}/s$, plasma frequency range from $w_p = 1.0\acute{}\ 10^{14}/s$ to $w_p = 1.0\acute{}\ 10^{16}/s$.

SI VI. Consistent Results across Multiple Devices

Transport measurements were performed to confirm that the optical modulation in layered materials related to the electronic states modulated with EDLG were consistent across multiple devices. Similar transfer characteristics (I_{DS}-V_G) of the Bi_2Se_3 nanoplates via the IL ([DEME]-[TFSI]) and ([EMIM]-[BF4]) gating effect are shown in S6 (a) and S6 (b), respectively.

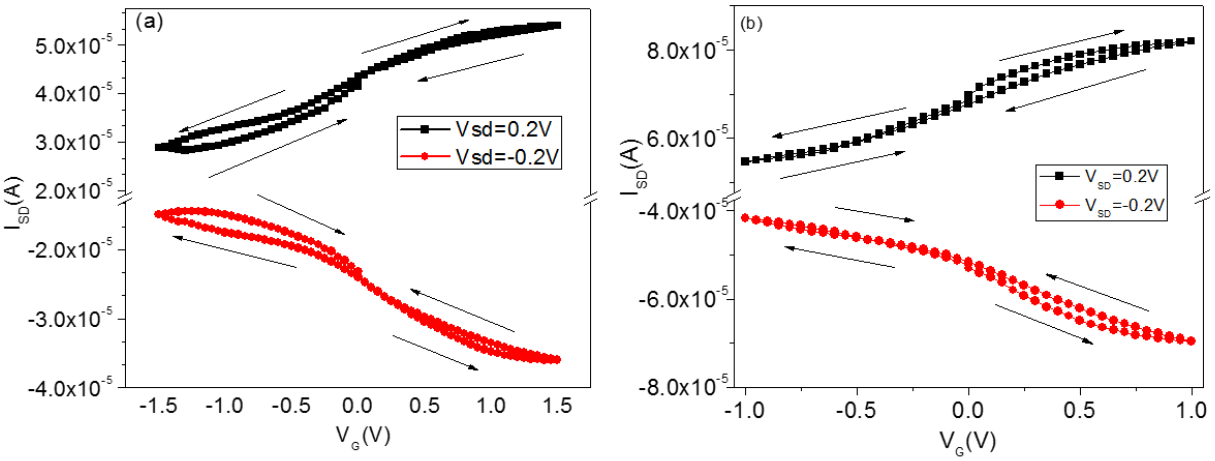

Supplementary **Figure S**6. Transfer characteristics (I_{DS}-V_G) of the Bi_2Se_3 nanoplates via IL **(a)** ([DEME]-[TFSI]) and **(b)** ([EMIM]-[BF4]) gating effect.

Supplementary References

1. Zhang, J.; Peng, Z. P.; Soni, A.; Zhao, Y. Y.; Xiong, Y.; Peng, B.; Wang, J. B.; Dresselhaus, M. S.; Xiong, Q. H. *Nano Lett* **2011,** 11, 2407-2414.
2. Zhou, K. G.; Withers, F.; Cao, Y.; Hu, S.; Yu, G. L.; Casiraghi, C. *Acs Nano* **2014,** 8, 9914-9924.

3. Tonndorf, P.; Schmidt, R.; Bottger, P.; Zhang, X.; Borner, J.; Liebig, A.; Albrecht, M.; Kloc, C.; Gordan, O.; Zahn, D. R. T.; de Vasconcellos, S. M.; Bratschitsch, R. *Opt Express* **2013,** 21, 4908-4916.
4. Hoff, R. M.; Irwin, J. C. *Phys Rev B* **1974,** 10, 3464-3470.
5. Peng, H. L.; Lai, K. J.; Kong, D. S.; Meister, S.; Chen, Y. L.; Qi, X. L.; Zhang, S. C.; Shen, Z. X.; Cui, Y. *Nat Mater* **2010,** 9, 225-229.
6. Marius Grundmann. The Physics of Semiconductors: An Introduction Including Devices and Nanophysics, Springer-Verlag Berlin Heidelberg, (2006).